Visual Abstract

Analysis of damage control of thin plate with piezoelectric actuators using finite element and machine learning approach

Asraar Anjum
Department of Mechanical and Aerospace Engineering, Faculty of Engineering, International Islamic University Malaysia, P.O. Box 10, 50725 Kuala Lumpur, Malaysia
asraar.anjum@live.iium.edu.my

Abdul Aabid
Department of Engineering Management, College of Engineering, Prince Sultan University, PO BOX 66833, Riyadh 11586, Saudi Arabia
aaabid@psu.edu.sa

Meftah Hrairi*
Department of Mechanical and Aerospace Engineering, Faculty of Engineering, International Islamic University Malaysia, P.O. Box 10, 50725 Kuala Lumpur, Malaysia
meftah@iium.edu.my

ABSTRACT. In recent studies, piezoelectric actuators have been recognized as a practical and effective material for repairing cracks in thin-walled structures, such as plates that are adhesively bonded with piezoelectric patches due to their electromechanical effects. In this study, we used the finite element method through the ANSYS commercial code to determine the stress intensity factor (SIF) at the crack tip of a cracked plate bonded with a piezoelectric actuator under a plane stress model. By running various simulations, we were able to examine the impact of different aspects that affect this component, such as the size and characteristics of the plate, actuator, and adhesive bond. To optimize performance, we utilized machine learning algorithms to examine how these characteristics affect the repair process. This study represents the first-time machine learning has been used to examine bonded PZT actuators in damaged structures, and we found that it had a significant impact on the current problem. As a result, we were able to determine which of these parameters were most helpful in achieving our goal and which ones should be adjusted to improve the actuator's quality and reduce significant time and costs.

KEYWORDS. Damaged structure, Piezoelectric actuators, Finite element method, Machine learning.

OPEN ACCESS

Citation: Anjum, A., Aabid, A., Hrairi, M., Analysis of damage control of thin plate with piezoelectric actuators using finite element and machine learning approach, Frattura ed Integrità Strutturale, 66 (2023) 112-126.

Received: 30.04.2023
Accepted: 02.08.2023
Online first: 05.08.2023
Published: 01.10.2023

INTRODUCTION

Many structural health monitoring researchers are interested in this topic because there is a rising need for an efficient, affordable, and trustworthy monitoring system to guarantee the functioning and safety of such structures [1–4]. Due to cyclic stresses and a corrosive operating environment, aircraft are susceptible to fracture over time. For example, fatigue cracks can form in corroded rivet holes and must be discovered and corrected before they cause catastrophic failure [5].

In early studies, damaged structures were studied by determining the fracture parameter such as stress intensity and stress concentration factor by using mathematical modelling [6] and the finite element method [7]. Later on, the same approach was used to compute SIF with bonded laminate structures [8,9]. After successfully computing the fracture parameter this continued with changing the parameter [10], damage propagation mode [11,12], and single/double-sided composite effects [13]. As an active repair method, the PZT was used to repair a notched beam under dynamic loading conditions by the electromechanical characteristic to induce a local moment [14]. With the use of PZT actuator patches, Wu and Wang [15] numerically and analytically restored the delaminated plate under uniaxial tensile strain. Dawood et al., [16] used LS-DYNA explicit FE code to explore delamination control in structures with PZT actuators by producing low-velocity impact. In recent studies, Aabid et al., [17] modelled the different repair configurations of a center-holed aluminium plate with a bonded PZT actuator. It has been determined stresses in a high-stress zone on a circular hole and repaired by increasing the voltage for a certain limit.

It suggests a system for quickly identifying and classifying concrete crack/non-crack features that combines picture binarization and a Fourier-based 1D DL model. DL training and testing using image binarization removes the plane structural backdrop and identifies potential Crack Candidate Regions (CCR) [18]. However, to regulate the centralised HVAC system of a multizone office complex, the heating, ventilation, and air conditioning (HVAC) system created a model-free end-to-end dynamic HVAC control approach based on a recently presented deep reinforcement learning framework [19]. It recommends utilising a simulated acceleration response on a nominal RC4 power car travelling over a 15m simply supported reinforced concrete railway bridge to train, test, and optimise a deep convolutional neural network to identify damage [20]. Similarly, to remotely gather thorough photos of road cracks, an omnidirectional mobile robot based on virtual reality technology is created. Next, a deep convolutional neural network (DCNN) model is trained and tested using an image dataset made up of various crack images gathered by the mobile robot [21]. And it introduces a piezoelectric sensor that uses frequency scanning technology and machine learning techniques to measure the thickness of ice and water coating on road surfaces. This sensor vibrates to identify ice and water using a constant elasticity alloy plate and a three-electrode piezoelectric transducer disc [22].

The tracking precision and robustness of traditional feedforward (FF) compensators against unmodeled dynamics and perturbation uncertainties were both increased by the reinforcement learning (RL) controller [23]. It introduces RL-Controller and proposes a revolutionary RL-based approach for creating active controllers. It suggests a framework that is simple to train for a benchmark building with five stories. In a study comparing the suggested model-free algorithm to the LQG active control approach, it is shown that the latter learns more effective actuator forcing schemes [24]. Case studies of damage detection of the model bridge and real bridge structures employing Digital twin (DT) technology or DL algorithms, with high accuracy of 92 percent, are used to show the viability of the suggested framework [25].

In the latest studies, piezoelectric materials adhesively bonded to structures were also found in some other cases such as in composite patches [26] which is used to evaluate the vibration excitation and separation in laminates and concrete beams which is used for damage evaluation of reinforced concrete structures at lap splices of tensional steel bars [27]. Additionally, the performance of PZT actuators was found in the effects of a viscoelastic bonding layer bonded to an elastic structure [28]. In some cases, surface-bonded piezoelectric sensors and actuators' performance on the host structures has been evaluated for PZT itself using FE simulations to check the adhesive layer effects, including non-uniform thickness [29]. However, no studies have been reported on reducing the crack damage propagation in a thin plate over the last four years of work excluding Aabid et al. [30] and Abuzaid et al. [31–35]. Therefore, the current study aims to reduce the SIF factor bonded with PZT actuators, and we introduce a novel methodology to determine the results through a machine learning approach. The study focuses on several parameters, including the position of the actuator, actuator cross-sectional area, actuator thickness, and adhesive thickness. To achieve this, we simulated various cases based on these parameters and levels, utilizing machine learning algorithms that have proven to be effective in this type of analysis. By identifying the most crucial factors that influence the result, we can improve actuator performance by determining its optimal size.

METHODOLOGY

Problem definition

A damaged rectangular plate with a piezoelectric actuator under uniform stress of 1 MPa is shown in Fig. 1. A thin-walled structure is utilized to simulate the current work. The distance of the actuator from the damaged edge affects the stress transmission to the crack surfaces because of the effectiveness of the repair. Therefore, given that the high stresses created by the integrated structure act at the piezoelectric actuator's edge, it is anticipated that the edge will be close to the fracture point [36]. The rectangular plate is 1 mm thick and has the following measurements: W = 40 mm, H = 200 mm. The plate features a 20 mm-long fracture that is open to an external load of 1 MPa. The actuator is 0.5 mm thick and measures Hp = 0.1H and 2Wp = 0.2H. The piezoelectric actuator is positioned at 1 mm from the crack tip and denoted as S. Tab. 1 lists the properties of the cracked plate, piezoelectric actuator, and adhesive bond.

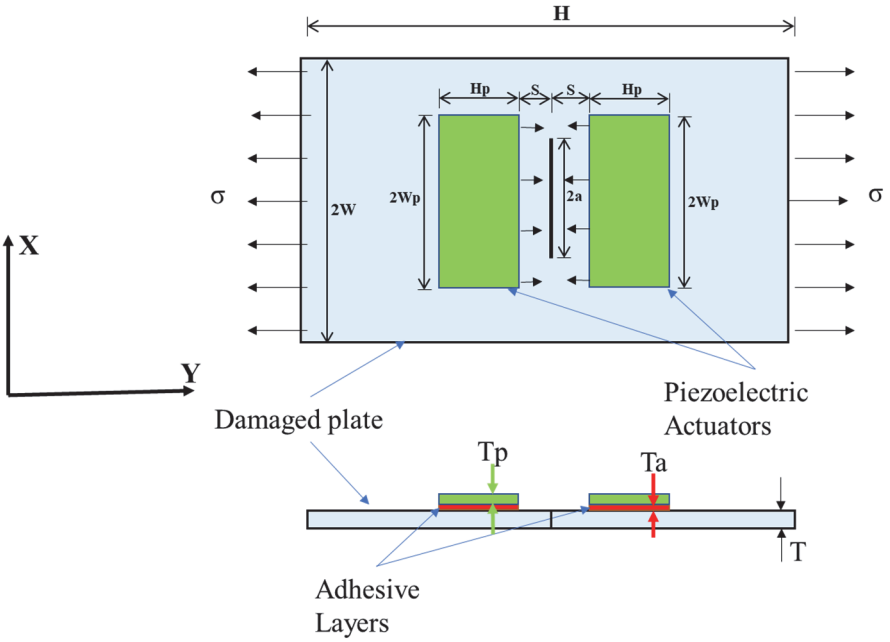

Figure 1: Center-cracked aluminum plate with piezoelectric actuators.

Parameter	Cracked Plate	PIC151 Patch	Adhesive
Density	2715 kg/m^3	7800 kg/m^3	1160 kg/m^3
Poisson's Ratio	0.33		0.345
Young's Modulus	68.95 GPa		5.1 GPa
Shear Modulus			1.2 GPa
Compliance Matrix	4	$S_{11} = 15.0\times10^{-12}$m^2/N $S_{33} = 19.0\times10^{-12}$m^2/N	
Electric Permittivity Coefficient	5	$\varepsilon_{11}^T = 1977$ $\varepsilon_{33}^T = 2400$	
PZT strain coefficient	9	$d_{31} = -2.10\times10^{-10}$m/V $d_{32} = -2.10\times10^{-10}$m/V	

Table 1: Properties of the cracked plate, PIC151, and adhesive.

Finite Element Simulation and Analysis

The present work employs a coupled-field analysis approach to investigate the interaction between structural and electric fields, with a specific focus on piezoelectric analysis. To model the piezoelectric actuator, we used the coupled element SOLID226 [37], which contains 20 nodes and can have up to 5 degrees of freedom. Meanwhile, the SOLID186 element

was used for the cracked plate and adhesive layer, a higher-order 20-noded element that is suited for solid structure analysis and recommended for linear application. To optimize run time and processor requirements, only one-quarter of the plate was considered due to symmetry, and a fine mesh was created around the fracture front to determine the SIF.
The interaction integral was employed to compute the SIF, using the virtual crack extension principles technique, which produced accurate results with fewer mesh requirements. To create a singularity in stresses and strains around the crack tip, singular elements were used, ideally oriented in the same direction as the crack. Fig. 2 displays the complete set of FE models for all aspects of the quarter model generated based on the given boundary conditions. The crack front was modelled using ten singular elements, while the PZT actuator was modelled using 4,999 coupled-field elements. The damaged plate was modelled using 12,393 high-order reduced integration solid elements, and the adhesive bond was modelled using 2,499 high-order reduced integration solid elements.

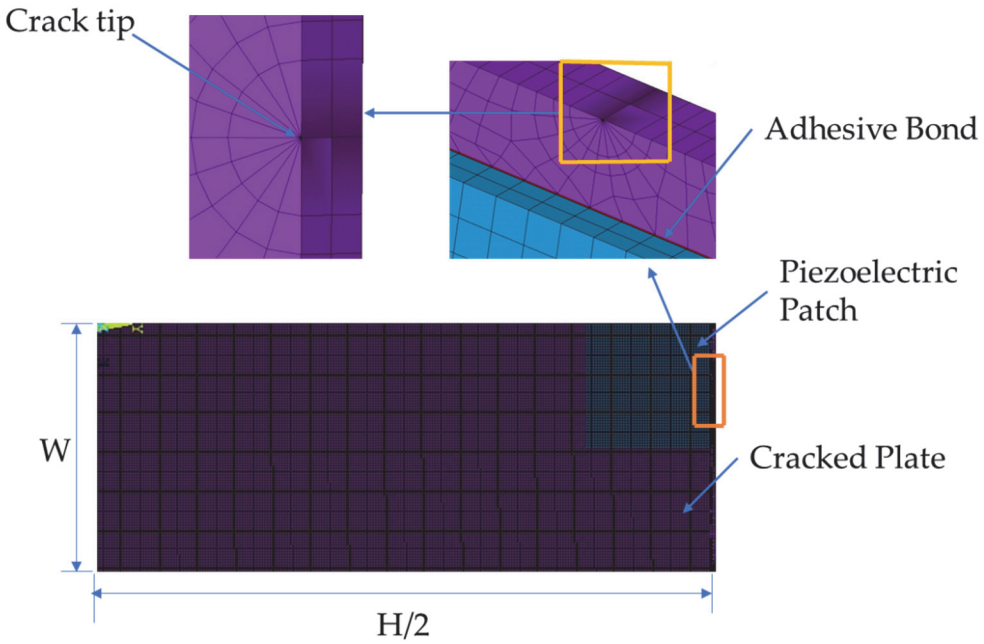

Figure 2. FE mesh model of the repaired plate.

Machine learning approach

Machine learning (ML) is a type of artificial intelligence that involves the use of algorithms to automatically learn from data, identify patterns, and make decisions without explicit instructions. ML is a powerful tool for data analysis that can automate the development of analytical models. However, there is no one-size-fits-all approach to using machine learning to solve real-world problems, as different problems require different methods. Fig. 3 provides an overview of the general process of using machine learning to analyses data.

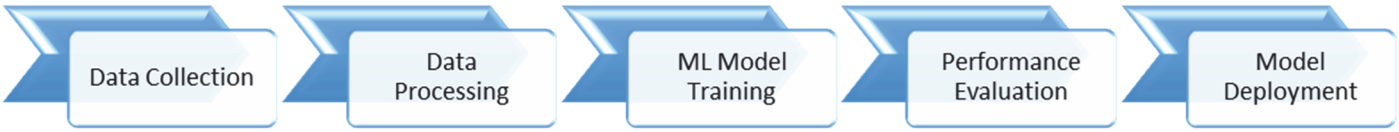

Figure 3. Machine Learning Process.

In this study, we examined the impact of actuator position, cross-sectional area, thickness, and adhesive thickness on the SIF using finite element simulations. Our dataset includes 4 features and 1 target value. Tab. 2 presents the features X1, X2, X3, and X4, which correspond to actuator position, cross-sectional area, thickness, and adhesive thickness, respectively. The target value, Y1, represents the SIF and is the goal parameter of our machine learning approach. Tab. 2 provides an overview of these characteristics and the desired values. We collected 27 data points through numerical simulations for our dataset.

Feature ID	Property	Notations	Levels	Range (mm)	Data type
X1	Position of Actuator	S	3	0.75 – 1.75	Numeric
X2	Actuator Cross-sectional Area	A	3	225 – 625	Numeric
X3	Actuator Thickness	Tp	3	0.5 – 1.0	Numeric
X4	Adhesive Thickness	Ta	3	0.0025 – 0.0035	Numeric

Table 2: Data set numerical model.

Selected machine learning models

Machine learning algorithms have become popular in solving problems in aeronautical, civil, and mechanical engineering due to their ability to predict optimal results using available information. In this study, FE results were used as input data and the objective was to reduce the SIF factor. Different variables such as dimensions and mechanical properties of the plate, adhesive bond, and bonded piezoelectric patch were chosen to achieve this objective. To predict the optimum results, Gaussian Process Regression (GPR) and Support Vector Machine (SVM) techniques with various kernel functions were implemented. The GPR is a probabilistic supervised machine learning framework that presents a probability distribution over potential functions that fit a set of points and computes the means and variances to show how confident the forecasts are [38]. The Gaussian processes model is a commonly used probabilistic framework in supervised machine learning for both classification and regression tasks. This model provides a probability distribution over a set of functions that can fit a given set of data points. By computing the means of these functions, we can obtain predictions for new data points, while variances provide a measure of confidence in these predictions, since they reflect the probability distribution over all possible functions [39].

Models based on the Gaussian process regression (GPR) kernel are nonparametric probabilistic models. Take into account the training set $\{(x_i, y_i); i = 1,2,...,n\}$, where $x_i \in \mathbb{R}^d$, and $y_i \in \mathbb{R}$, are taken from an unidentified distribution. With the fresh input vector $xnew$ and the training data, a GPR model attempts to predict the value of a response variable $ynew$. The formula for a linear regression model is

$$y = x^T \beta + \varepsilon,$$

where $\varepsilon \sim N(0, \sigma^2)$. The coefficients β and error variance σ^2 are estimated using the data. A GPR model uses explicit basis functions, h , and latent variables, $f(x_i), i = 1,2,...,n,$ from a Gaussian process (GP), to describe the response. The smoothness of the response is captured by the covariance function of the latent variables, and basic functions project the inputs x into a p-dimensional feature space [40,41].

A GP is a collection of random variables that all have the same joint Gaussian distribution for any finite number of them. Given n observations $(x1, x2, ..., xn,)$, the joint distribution of the random variables $(f(x1), f(x2), ..., f(xn))$ is Gaussian if $\{f(x), x \in \mathbb{R}^d\}$ is a GP. A GP is described by its covariance function, k (x, x '), and mean function, m(x). In other words, if the function $\{f(x), x \in \mathbb{R}^d\}$ is a Gaussian process, then $E(f(x)) = m(x)$ and $Cov[f(x), f(x')] = E[\{f(x) - m(x)\}\{f(x') - m(x')\}] = k(x, x')$.

The Gaussian model is represented by

$$h(x)T\beta + f(x)$$

where $f(x) \sim GP(0, k(x, x'))$ indicates that $f(x)$ are from a zero mean GP with covariance function, $k(x, x')$. x in $\mathbb{R}^d$ is changed into the new feature vector $h(x)$ in R^p by a collection of basis functions called $h(x)$. A basis function coefficients vector of size p by 1 is known as β .

One way to model a response y instance is as

$$P\left(yi \mid f\left(x_i\right), x_i\right) \sim N\left(y_i \mid h\left(x_i\right) T\beta + f\left(x_i\right), \sigma 2\right)$$

Therefore, a GPR model is a probabilistic model. The GPR model is nonparametric since a latent variable $f\left(x_i\right)$ is introduced for each observation x_i.

In the GPR model, the latent variables $\left(x1\right), f\left(x2\right), ..., f(xn$ have the following joint distribution:

$$P\left(f \mid X\right) \sim N\left(f \mid 0, K\left(X, X\right)\right),$$

which resembles a linear regression model, where $K\left(X, X\right)$

$$K\left(X, X\right) = \begin{pmatrix} & & & \\ k\left(x1, x1\right) & k\left(x1, x2\right) & \cdots & k\left(x1, xn\right) \\ k\left(x2, x1\right) & k\left(x2, x2\right) & \cdots & k\left(x2, xn\right) \\ \vdots & \vdots & & \vdots \\ k\left(xn, x1\right) & k\left(xn, x2\right) & \cdots & k\left(xn, xn\right) \end{pmatrix}$$

Typically, a set of kernel parameters or hyperparameters, θ are used to parameterize the covariance function $k\left(x, x'\right)$ and is frequently written as $k\left(x, x' \mid \theta\right)$ to explicitly state the reliance on θ.

The kernel parameters are based on the signal standard deviation σf and the characteristic length scale σl for many of the standard kernel functions. The characteristic length scales provide a brief definition of the minimum distance at which the input values xi must be separated before the response values become uncorrelated. The various kernel functions used in this study are listed in Tab. 3.

Kernel Function	Covariance function definition
Rational Quadratic Kernel	$k\left(x_i, x\mathrm{j} \mid \theta\right) = \sigma_f^2 \left(1 + \frac{r^2}{2\alpha\sigma_l^2}\right)^{-\alpha}$
Matern 5/2 GPR	$k\left(x\mathrm{i}, x\mathrm{j}\right) = \sigma_f^2 \left(1 + \frac{\sqrt{5}r}{\sigma_l} + \frac{5r^2}{3\sigma_l^2}\right) \exp\left(-\frac{\sqrt{5}r}{\sigma_l}\right)$
Exponential GPR	$k\left(x\mathrm{i}, x\mathrm{j} \mid \theta\right) = \sigma_f^2 \ \exp\left(-\frac{r}{\sigma_l}\right)$
Squared Exponential GPR	$k\left(x\mathrm{i}, x\mathrm{j} \mid \theta\right) = \sigma_f^2 \ \exp\left[-\frac{1}{2}\frac{\left(x_i - x_j\right)^T \left(x_i - x_j\right)}{\sigma_l^2}\right]$

Table 3. Kernel functions for the GPR technique [37].

where $r = \sqrt{\left(x_i - x_j\right)^T \left(x_i - x_j\right)}$ is the Euclidean distance between x_i and x_j and α is a positive-valued scale-mixture parameter.

Vladimir Vapnik and his coworkers reported the support vector machine (SVM) analysis in 1992 [42], and it has since become a widely used machine learning technique for classification and regression. As a result of its reliance on kernel functions, SVM regression is regarded as a nonparametric method. There are various kernel functions available for SVM techniques as shown in Tab. 4. In this study, polynomial kernel functions with order 2 and order 3 are used.

The performance of regression models is evaluated using various evaluation metrics such as root means square error (RMSE), mean absolute error (MAE), mean absolute percentage error (MAPE) and coefficient of determination (R^2). The mathematical formulations, characteristics, applications, advantages, disadvantages, and limitations of these metrics can be found in [43].

Type of SVM	Mercer Kernel	Description
Gaussian or Radial Basis Function (RBF)	$k(x_1,x_2)=\exp\left(-\frac{x_1-x_2^{\,2}}{2\sigma^2}\right)$	One class learning. σ is the width of the kernel
Linear	$k(x_1,x_2)=x_1^T x_2$	Two class learning.
Polynomial	$k(x_1,x_2)=\left(x_1^T x_2+1\right)^{\rho}$	ρ is the order of the polynomial
Sigmoid	$k(x_1,x_2)=\tanh\left(\beta_0 x_1^T x_2+\beta_1\right)$	β_0, and β_1 are constants for which it becomes a mercer kernel function.

Table 4. Types of SVM and Kernel Functions [41].

FINITE ELEMENT RESULTS AND DISCUSSION

Grid independence test

To evaluate the influence of mesh size on computational results, three mesh sizes were chosen and presented in Fig. 4. The adhesive bond and piezoelectric actuator were meshed using the grid-structured mesh with component size based on the mesh type. The elements were separated for the damaged plate by choosing each line, resulting in an unstructured type of mesh. As shown in Fig. 4, refining the mesh from medium to fine led to a slight improvement in the accuracy of the SIF value solution, with a maximum relative difference of 14 percent. However, the medium mesh provided adequate resolution and accuracy while requiring only half the computation time, making it the preferred option for the remaining simulations.

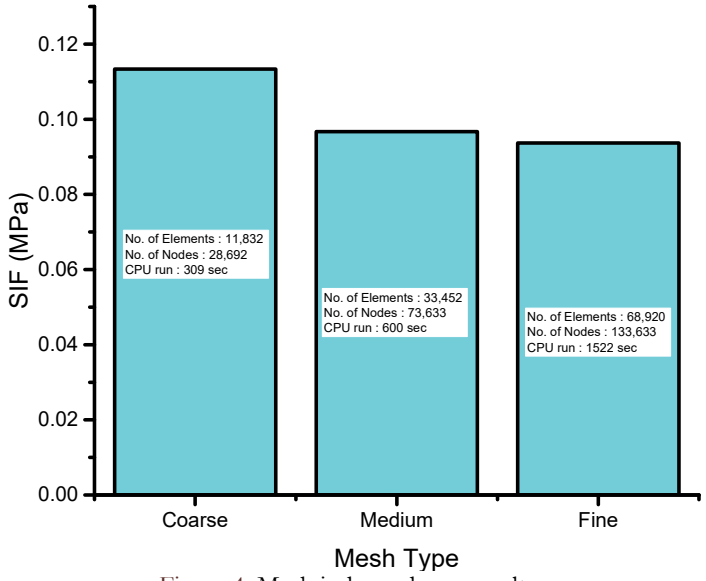

Figure 4: Mesh independence results.

Validation of the numerical model

Fig. 5 provides visual evidence of the strong agreement between the two results, indicating that the computational model is a reliable and accurate representation of the physical experiment. The maximum relative error of about 10% suggests that the differences between the simulation and experimental results are relatively small, considering the complexities involved in conducting physical experiments. Despite the small differences, it is important to note that the accuracy of the experimental results may have been affected by various factors, such as human error in situating and aligning the

piezoelectric actuator and strain gage on the host plate. These challenges can lead to variations in the experimental results, which may not be present in the simulation results. Additionally, the small notch outside the computational model that initiates the crack may have had an impact on the experimental results. The presence or absence of such factors could explain the minor differences between the two sets of results. Overall, the linear fluctuation of the SIF with the applied electric field remains consistent with the supersession principles, providing further support for the accuracy of the computational model.

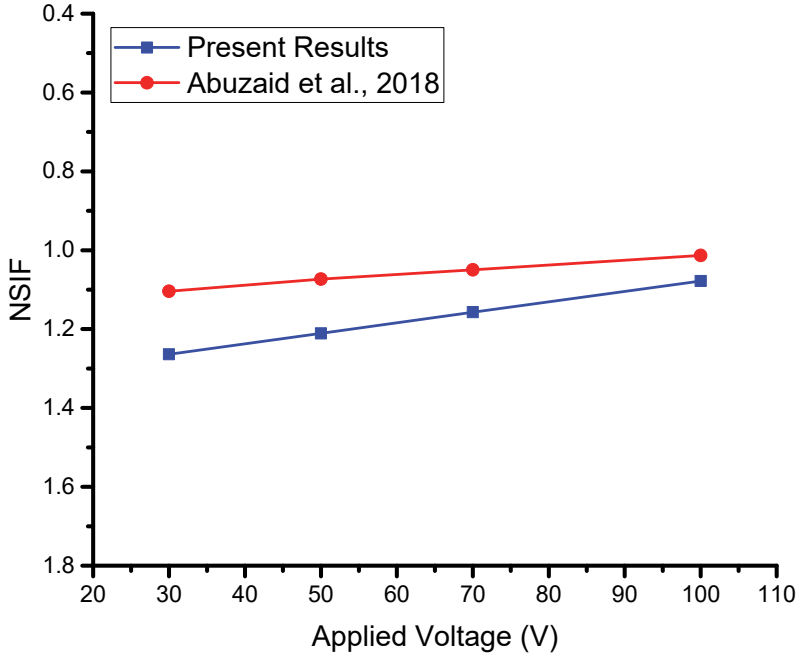

Figure 5: Validation of current FE findings using experimental data from [31].

Reduction of stress intensity factor

The study presented in Fig. 6 shows the reduction in SIF for the patched plate in comparison to the unpatched plate. Based on results it shows SIF decreases linearly with the increase in crack length. The plot represents the maximum reduction of applied negative voltage at 150 V [31]. As the crack length decreases, it was observed that the SIF increases and the percentage reduction falls. This is due to the requirement of a greater negative electric field to decrease the SIF to the same level for shorter crack lengths, owing to the larger stress gradient in the crack tip region. For instance, a voltage of 150 V applied to a crack length of 5 mm resulted in a reduction of approximately 52.3% in the SIF, while a crack length of 12.5 mm resulted in a reduction of only 45.8%.

The observed linear relationship between the crack length and the reduction of SIF is an essential finding that can help researchers design more effective patch configurations to reduce SIF in practical applications. The results also suggest that the effectiveness of the patch decreases as the crack length reduces, indicating that the patch's ability to mitigate damage is more effective for larger cracks. However, it should be noted that the reduction in SIF is not the only factor to consider in practical applications, and other factors such as the cost, weight, and durability of the patch should also be considered in the design process. Overall, the findings from this study provide valuable insights into the use of piezoelectric patches for reducing SIF in damaged structures.

MACHINE LEARNING RESULTS AND DISCUSSION

In the current study, six different models were used to predict the results (Tab. 5) using the regression learner app of release 2022a of MATLAB® [44]. Simulated FE results are predicted using six machine-learning models. Fig. 7 shows the responses using various methods, Fig. 8 shows the comparison of true response vs the predicted response by various models and Fig. 9 shows residuals of various models. Tab. 6 provides the simulated values vs the predicted values for each parametric variation. From Fig. 10 model 3 and model 6 give us the best fit, which results in lower RMSE values and R^2 values nearer to 1.

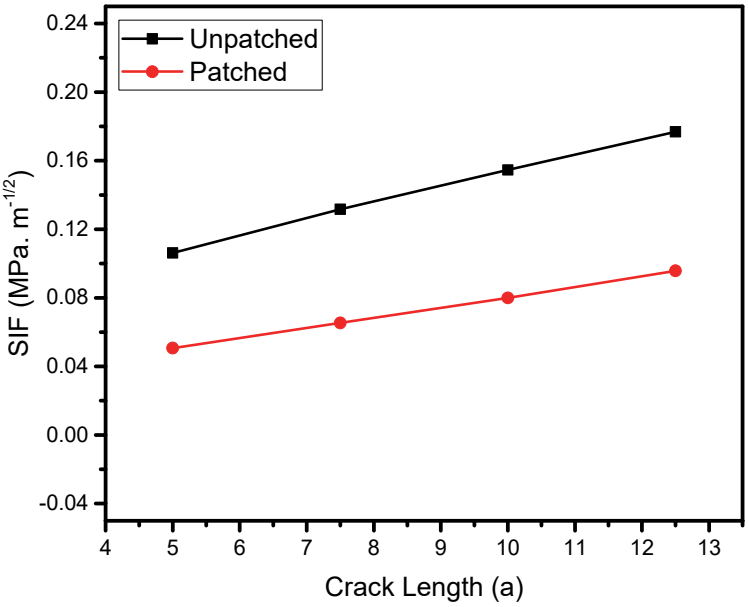

Figure 6. Comparison of patched and unpatched plates.

Model Number	Model	Model Parameters
Model 1	Quadratic SVM	Kernel function-Polynomial; Kernel polynomial order-2; Solver-Sequential Minimal Optimization; Epsilon-0.005
Model 2	Cubic SVM	Kernel function-Polynomial; Kernel polynomial order-3; Solver-Sequential Minimal Optimization; Epsilon-0.005
Model 3	Rational Quadratic GPR	Kernel function-Rational Quadratic; Optimizer-Quasi Newton; Method – Gaussian Process Regression
Model 4	Matern 5/2 GPR	Kernel function-Matern 5/2; Optimizer-Quasi Newton; Method – Gaussian Process Regression
Model 5	Exponential GPR	Kernel function- Exponential; Optimizer-Quasi Newton; Method – Gaussian Process Regression
Model 6	Squared Exponential GPR	Kernel function-Squared Exponential; Optimizer-Quasi Newton; Method – Gaussian Process Regression

Table 5. Model descriptions.

Finite element simulations require a mesh study to achieve accurate results. Typically, a fine mesh is preferred for accurate results. After conducting mesh sensitivity analysis, a fine mesh was chosen for this study. As a result, the FE and ML work achieved less than a 1% error, which can be safely ignored. Furthermore, the selected ML models were found to be suitable for predicting and simplifying the current problem. Therefore, this simulation demonstrates that the selected ML models can accurately predict and simplify the current problem.

Fig. 7 demonstrates the performance of the GPR and SVM algorithms in predicting the SIF values. Both training and testing results using GPR and SVM algorithms are presented, and the predicted values are compared to the simulation data for the respective data sets. The results reveal that the GPR algorithm using Rational Quadratic and Squared Exponential kernel functions is effective in predicting the SIF values for these data sets, and the algorithm fits well with the simulation data. The GPR algorithm was further optimized to fit the validation samples with the simulation data, which resulted in good agreement with the FE data for the tested data. This study is noteworthy as it is the first to utilize six different regression models for the regression analysis of solid mechanics and structure problems. Additionally, this study highlights the potential of GPR for the analysis of highly linear and non-linear numeric data, as the results indicate that the SIF values are significantly dependent on the patch shear strength, which was successfully predicted by GPR for the testing points. This study demonstrates the potential of GPR for various fields where regression analysis of highly linear and non-linear numeric data is required.

The comparison of the regression results of SIF using GPR and SVM algorithms is important for predicting the values of the data sets with high accuracy. The Rational Quadratic and Squared Exponential kernel functions used in the GPR algorithm prove to be effective in predicting the data sets and fitting properly with simulation results. This study provides valuable insight into the potential of GPR for regression analysis in the field of solid mechanics and structure problems. Furthermore, the successful prediction of the testing points by GPR demonstrates its suitability for highly non-linear data analysis. The study's novelty lies in its comprehensive comparison of six different regression models, paving the way for future research to explore GPR on topics with highly linear and non-linear numeric data.

Runs	Simulation Response Output	NSIF using Machine Learning Techniques					
	NSIF	Model 1	Model 2	Model 3	Model 4	Model 5	Model 6
1	0.443706	0.464191	0.448939	0.446833	0.449311	0.46889	0.446833
2	0.519506	0.512213	0.514377	0.519338	0.519317	0.519487	0.519338
3	0.57479	0.567337	0.570027	0.574677	0.574723	0.574755	0.574677
4	0.422777	0.450991	0.428494	0.423224	0.423039	0.422836	0.423224
5	0.473577	0.496179	0.480527	0.473615	0.473723	0.473615	0.473615
6	0.504582	0.508822	0.510129	0.504501	0.504626	0.504598	0.504501
7	0.43676	0.436135	0.434291	0.436658	0.436658	0.43676	0.436658
8	0.465967	0.460134	0.461338	0.465924	0.465922	0.465959	0.465924
9	0.48866	0.493809	0.490649	0.488752	0.488685	0.488668	0.488752
10	0.479372	0.48213	0.482995	0.479456	0.479428	0.479393	0.479456
11	0.548186	0.529621	0.540968	0.548162	0.548245	0.548157	0.548162
12	0.598832	0.584213	0.592897	0.599111	0.598931	0.598808	0.599111
13	0.453232	0.46596	0.458793	0.45266	0.45299	0.453236	0.45266
14	0.498066	0.510617	0.502352	0.49811	0.498004	0.498083	0.49811
15	0.526072	0.528489	0.530316	0.526229	0.526055	0.526076	0.526229
16	0.464992	0.447835	0.454094	0.458952	0.454308	0.449011	0.458952
17	0.489278	0.477063	0.484282	0.489563	0.489619	0.480984	0.489563
18	0.508227	0.510206	0.505695	0.508132	0.508204	0.508224	0.508132
19	0.505432	0.500228	0.509872	0.505389	0.505418	0.50543	0.505389
20	0.570027	0.547188	0.563585	0.569952	0.569883	0.569986	0.569952
21	0.617714	0.601249	0.614996	0.617507	0.617621	0.617659	0.617507
22	0.474824	0.481089	0.480268	0.475108	0.474972	0.474852	0.475108
23	0.516393	0.525215	0.518556	0.516504	0.516516	0.516426	0.516504
24	0.542765	0.548315	0.548186	0.5428	0.542863	0.542775	0.5428
25	0.484435	0.459694	0.462965	0.473563	0.465459	0.468738	0.473563
26	0.50605	0.49415	0.499598	0.506002	0.505987	0.506027	0.506002
27	0.523015	0.526763	0.516317	0.521929	0.522337	0.525415	0.521929

Table 6. Machine learning outcomes.

The residual is the difference between the predicted value and the actual value, and Fig. 8 displays the residual plots for different models. A negative residual value indicates that the predicted value is greater than the actual value, while a positive residual value suggests that the predicted value is less than the actual value. As depicted in Fig. 8, model 3 and model 8 demonstrate the best fit for the dataset. The regression line for the given data with an R-Square value of 0.998 is shown in Fig. 8. To ensure the accuracy of the regression models, it is essential to evaluate the residual plot. The residual plot helps to identify the outliers and the presence of patterns in the data. From the residual plot in Fig. 9, it is observed that model 3 and model 8 have the lowest values of residuals, indicating that they have the best fit to the data. In contrast, models 1, 2, 4, 5, 6, and 7 have higher residuals, which indicates a less accurate fit to the data. The R-Square value of 0.998 for the regression line in Fig. 9 indicates that the regression models have a high degree of fit to the data. Overall, the residual plot and R-Square value suggest that models 3 and 8 are the most appropriate regression models for the given dataset.

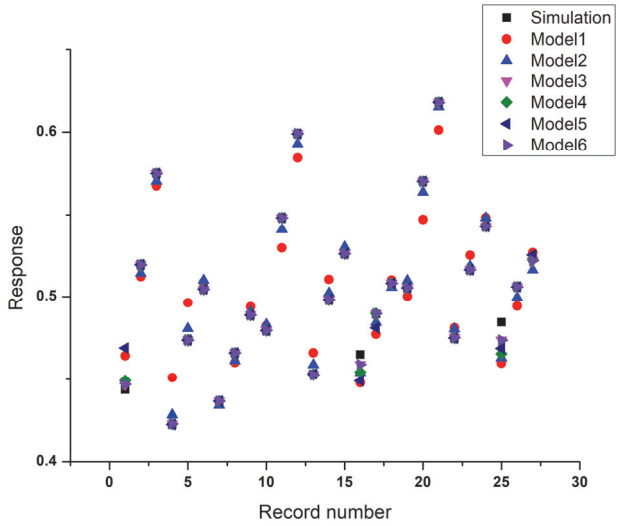

Figure 7: Comparison of responses using various methods.

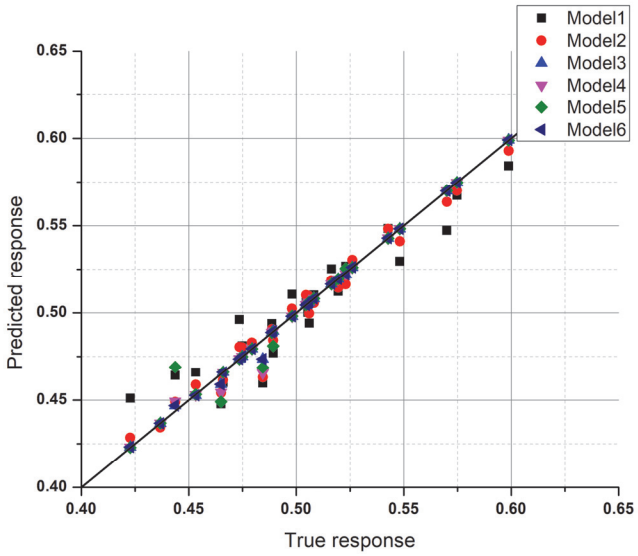

Figure 8: True response vs the predicted.

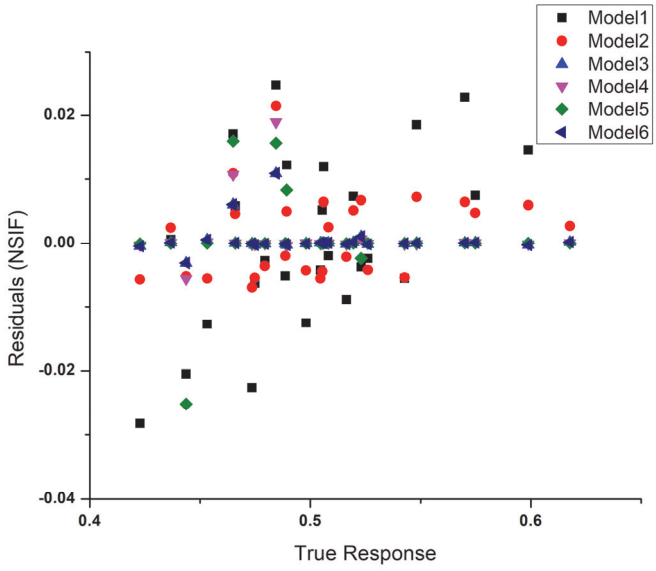

Figure 9: True response vs the residual.

Fig. 10 illustrates the evaluation metrics for the six different models used in this study. The metrics include MAE (Mean Absolute Error), MAPE (Mean Absolute Percentage Error), RMSE (Root Mean Squared Error), and R-Square values. From the results, it is observed that model 3 and model 6 exhibit the least values of MAE, MAPE, and RMSE, with the highest R-Square value of 0.997377. These values indicate that these two models have the same accuracy and performance. Conversely, model 1 is found to be the least accurate model among the six models used in the study, with an RMSE of 0.013593. Overall, the evaluation metrics demonstrate that models 3 and 6 perform better than the other models in predicting the outcomes.

The evaluation metrics presented in Fig. 10 provide insight into the performance of the different models. The results indicate that models 3 and 6 performed the best among the six models tested. These two models have the lowest values of MAE, MAPE, and RMSE, and the highest value of R-square. The low values of MAE, MAPE, and RMSE suggest that these models have less error and better accuracy in predicting the outcomes. Moreover, the high value of R-square indicates that these models have a strong correlation between the predicted and actual values. Conversely, model 1 had the least accuracy among all six models, with a higher value of RMSE. The results presented in Tab. 7 support the findings of Fig. 10, indicating that models 3 and 6 are the most accurate models in predicting the outcomes of interest. These findings suggest that models 3 and 6 could be preferred over other models for predicting the outcomes in this study.

Machine Learning Algorithm Applied	R-Squared	RMSE
Quadratic SVM	0.92406	0.013593
Cubic SVM	0.98045	0.006714
Rational Quadratic GPR	0.99738	0.002484
Matern 5/2 GPR	0.99209	0.004331
Exponential GPR	0.97993	0.006696
Squared Exponential GPR	0.99738	0.002484

Table 7: Comparison of Evaluation metrics for various regression models.

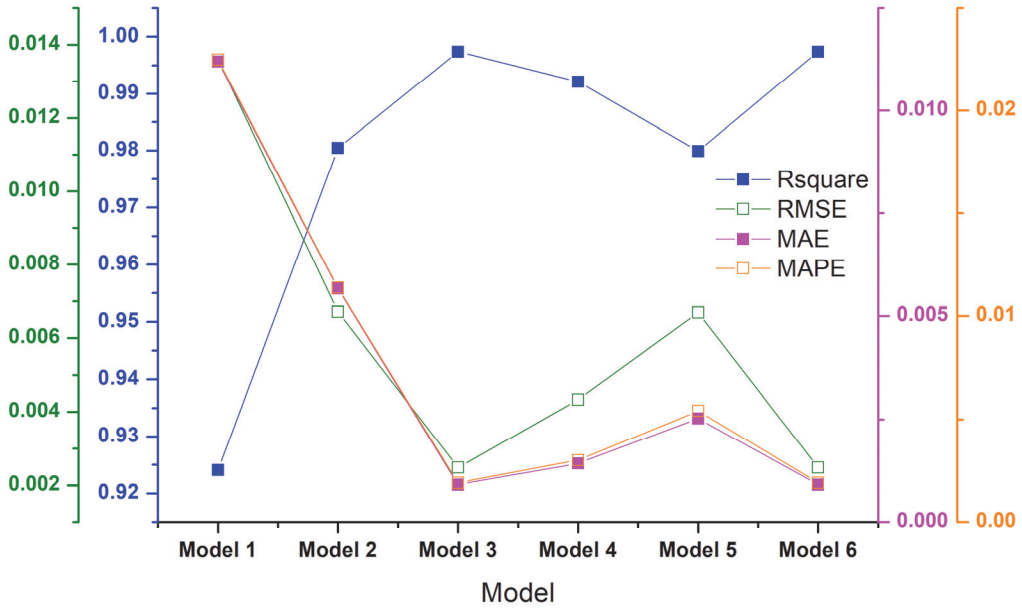

Figure 10. Various evaluation metrics for different models.

Conclusion

The study presented a successful approach for identifying the optimal value of SIF for damage control in an aluminum thin plate structure. To achieve this, 27 finite element simulations were performed with varying parameters, and six machine learning models were utilized to predict the SIF. The finite element method was initially used to obtain SIF with four different parameters and three different levels as input parameters/levels. The results showed that machine

learning algorithms are an effective and practical approach to understanding complex phenomena as they consider all components and their interactions. Furthermore, the method allowed for the identification of the actuators and adhesive parameters that resulted in the lowest SIF, and consequently, the enhancement of the actuator design. This study contributes to the advancement of the understanding and control of SIF in thin plate structures and highlights the potential of machine learning in solid mechanics and structural engineering.

Acknowledgement

The author Asraar Anjum acknowledges the support of the TFW2020 scheme from the Kulliyyah of Engineering, International Islamic University Malaysia and this research was supported by the Ministry of Education of Malaysia (MOE) through Fundamental Research Grant Scheme (FRGS/1/2021/TK0/UIAM/01/5). Also, the authors acknowledge the support of the Structures and Materials (S&M) Research Lab of Prince Sultan University.

Conflicts of interest

The authors declare no conflict of interest.

Availability of data and materials

The datasets used during the current study are available from the corresponding author upon reasonable request.

References

[1] Aabid, A., Baig, M., Hrairi, M. (2023). Advanced Composite Materials for Structural Maintenance, Repair, and Control, Materials (Basel)., 16(2), pp. 743.

[2] Aabid, A., Parveez, B., Raheman, M.A., Ibrahim, Y.E., Anjum, A., Hrairi, M., Parveen, N., Zayan, J.M. (2021). A review of piezoelectric materials based structural control and health monitoring techniques for engineering structures : challenges and opportunities, Actuators, 10(5), pp. 101, Doi: https://doi.org/10.3390/ act10050101.

[3] Aabid, A., Raheman, A., Ibrahim, Y.E., Anjum, A., Hrairi, M., Parveez, B., Parveen, N., Zayan, J.M. (2021). A Systematic Review of Piezoelectric Materials and Energy Harvesters for Industrial Applications, Sensors, 21, pp. 1–28, Doi: https://doi.org/10.3390/s21124145.

[4] Aabid, A., Hrairi, M., Mohamed Ali, S.J., Ibrahim, Y.E. (2023). Review of Piezoelectric Actuator Applications in Damaged Structures: Challenges and Opportunities, ACS Omega, 8, pp. 2844–60, Doi: 10.1021/acsomega.2c06573.

[5] Jones, R., Molent, L., Pitt, S. (1999). Study of multi-site damage of fuselage lap joints, Theor. Appl. Fract. Mech., 32(2), pp. 81–100, DOI: 10.1016/S0167-8442(99)00029-4.

[6] Bueckner, H.F. (1970). A novel principle for the computation of stress intensity factors, Akad. GmbH, 50(9), pp. 529–546.

[7] Henshell, R.D., K.G. Shaw. (1975). Crack Tip Finite Element are Unnecessary, Int. J. Numer. Methods Eng., 9, pp. 495–507.

[8] Ratwani, M. (1979). Analysis of cracked, adhesively bonded laminated structures, AIAA J., 17(9), pp. 988–994, DOI: 10.2514/3.61263.

[9] Rose, L.R.F. (1982). A cracked plate repaired by bonded reinforcements, Int. J. Fract., 18(2), pp. 135–144, DOI: 10.1007/BF00019638.

[10] Bassetti, A., Colombi, P., Nussbaumer, a. (2000). Finite Element Analysis of Steel Members Repaired By Prestressed Composite Patch, Convegno IGF 15, , pp. 1–10.

[11] Bouiadjra, B.B., Belhouari, M., Serier, B. (2002). Computation of the stress intensity factors for repaired cracks with bonded composite patch in mode I and mixed mode, Compos. Struct., 56, pp. 401–406.
[12] Megueni, A., Bouiadjra, B.B., Boutabout, B. (2003). Computation of the stress intensity factor for patched crack with bonded composite repair in pure mode II, Compos. Struct., 59, pp. 415–418.
[13] Belhouari, M., Bouiadjra, B.B., Megueni, A., Kaddouri, K. (2004). Comparison of double and single bonded repairs to symmetric composite structures : a numerical analysis, Compos. Struct., 65, pp. 47–53, DOI: 10.1016/j.compstruct.2003.10.005.
[14] Wang, Q., Duan, W.H., Quek, S.T. (2004). Repair of notched beam under dynamic load using piezoelectric patch, Int. J. Mech. Sci., 46(10), pp. 1517–1533, DOI: 10.1016/j.ijmecsci.2004.09.012.
[15] Wu, N., Wang, Q. (2010). Repair of a delaminated plate under static loading with piezoelectric patches, Smart Mater. Struct., 19(10), pp. 105025, DOI: 10.1088/0964-1726/19/10/105025.
[16] Shaik Dawood, M.S.I., Iannucci, L., Greenhalgh, E., Ariffin, A.K. (2012). Low Velocity Impact Induced Delamination Control Using MFC Actuator, Appl. Mech. Mater., 165, pp. 346–51, DOI: 10.4028/www.scientific.net/AMM.165.346.
[17] Aabid, A., Hrairi, M., Dawood, M.S.I.S. (2019). Modeling Different Repair Configurations of an Aluminum Plate with a Hole, Int. J. Recent Technol. Eng., 7(6S), pp. 235–240.
[18] Kolappan Geetha, G., Sim, S.H. (2022). Fast identification of concrete cracks using 1D deep learning and explainable artificial intelligence-based analysis, Autom. Constr., 143, pp. 104572, DOI: 10.1016/j.autcon.2022.104572.
[19] Zhong, X., Zhang, Z., Zhang, R., Zhang, C. (2022). End-to-End Deep Reinforcement Learning Control for HVAC Systems in Office Buildings, Designs, 6(3), DOI: 10.3390/designs6030052.
[20] Hajializadeh, D. (2022). Deep-Learning-Based Drive-by Damage Detection System for Railway Bridges, Infrastructures, 7(6), DOI: 10.3390/infrastructures7060084.
[21] Zhu, G., Fan, Z., Ma, P., Huang, W., Ye, Z., Huang, M., Li, J., Jiang, Z., Zhong, Z., He, W. (2021). Road Crack Acquisition and Analysis System Based on Mobile Robot and Deep Learning, 2021 IEEE 11th Annu. Int. Conf. CYBER Technol. Autom. Control. Intell. Syst. CYBER 2021, pp. 601–7, DOI: 10.1109/CYBER53097.2021.9588151.
[22] Gui, K., Ge, J., Ye, L., Huang, L. (2019). The piezoelectric road status sensor using the frequency scanning method and machine-learning algorithms, Sensors Actuators, A Phys., 287, pp. 8–20, DOI: 10.1016/j.sna.2018.12.048.
[23] Li, N., Tang, J., Li, Z.X., Gao, X. (2022). Reinforcement learning control method for real-time hybrid simulation based on deep deterministic policy gradient algorithm, Struct. Control Heal. Monit., 29(10), DOI: 10.1002/stc.3035.
[24] Eshkevari, S.S., Eshkevari, S.S., Sen, D., Pakzad, S.N. (2021). RL-Controller: a reinforcement learning framework for active structural control. DOI: 10.48550/arXiv.2103.07616
[25] Dang, H., Tatipamula, M., Nguyen, H.X. (2022). Cloud-Based Digital Twinning for Structural Health Monitoring Using Deep Learning, IEEE Trans. Ind. Informatics, 18(6), pp. 3820–3830, DOI: 10.1109/TII.2021.3115119.
[26] Her, S.C., Chen, H.Y. (2022). Vibration Excitation and Suppression of a Composite Laminate Plate Using Piezoelectric Actuators, Materials (Basel), 15(6), DOI: 10.3390/ma15062027.
[27] Regupathi, R., Jayaguru, C. (2022). Damage Evaluation of Reinforced Concrete structures at lap splices of tensional steel bars using Bonded Piezoelectric Transducers, Lat. Am. J. Solids Struct., 19(3), pp. 1–15, DOI: 10.1590/1679-78257069.
[28] Ali, I.A., Alazwari, M.A., Eltaher, M.A., Abdelrahman, A.A. (2022). Effects of viscoelastic bonding layer on performance of piezoelectric actuator attached to elastic structure, Mater. Res. Express, 9(4), DOI: 10.1088/2053-1591/ac5cae.
[29] Velásquez, J.Q., Trindade, M.A. (2021). Finite element modeling and analysis of adhesive layer effects in surface-bonded piezoelectric sensors and actuators including non-uniform thickness, Mech. Adv. Mater. Struct., 0(0), pp. 1–16, DOI: 10.1080/15376494.2021.1907490.
[30] Aabid, A., Hrairi, M., Abuzaid, A., Mohamed Ali, J.S. (2021). Estimation of stress intensity factor reduction for a center-cracked plate integrated with piezoelectric actuator and composite patch, Thin-Walled Struct., 158, DOI: 10.1016/j.tws.2020.107030.
[31] Abuzaid, A., Hrairi, M., Dawood, M.S. (2017). Modeling approach to evaluating reduction in stress intensity factor in center-cracked plate with piezoelectric actuator patches, J. Intell. Mater. Syst. Struct., 28(10), pp. 1334–1345, DOI: 10.1177/1045389X16672562.
[32] Abuzaid, A., Hrairi, M., Dawood, M.S. (2015). Mode I Stress Intensity Factor for a Cracked Plate with an Integrated Piezoelectric Actuator, Adv. Mater. Res., 1115, pp. 517–22, DOI: 10.4028/www.scientific.net/AMR.1115.517.
[33] Abuzaid, A., Dawood, M.S., Hrairi, M. (2015). Effects of Adhesive Bond on Active Repair of Aluminium Plate Using Piezoelectric Patch, Appl. Mech. Mater., 799–800, pp. 788–93, DOI: 10.4028/www.scientific.net/AMM.799-800.788.
[34] Abuzaid, A., Hrairi, M., Dawood, M. (2018). Evaluating the Reduction of Stress Intensity Factor in Center-Cracked Plates Using Piezoelectric Actuators, Actuators, 7(2), pp. 25, DOI: 10.3390/act7020025.

[35] Abuzaid, A., Hrairi, M., Dawood, M.S. (2018). Experimental and numerical analysis of piezoelectric active repair of edge-cracked plate, J. Intell. Mater. Syst. Struct., 29(18), pp. 3656–66, DOI: 10.1177/1045389X18798949.
[36] Crawley, E.F., De Luis, J. (1987). Use of piezoelectric actuators as elements of intelligent structures, AIAA J., 25(10), pp. 1373–1385, DOI: 10.2514/3.9792.
[37] ANSYS Inc. (2017). ANSYS FLUENT 18.0: Theory Guidance, Canonsburg PA.
[38] Aabid, A., Hrairi, M., Abuzaid, A., Syed, J., Ali, M. (2021). Estimation of stress intensity factor reduction for a center-cracked plate integrated with piezoelectric actuator and composite patch, Thin-Walled Struct., 158, pp. 107030, DOI: 10.1016/j.tws.2020.107030.
[39] Wang, J. (2020). An Intuitive Tutorial to Gaussian Processes Regression, DOI: 10.48550/arXiv.2009.10862
[40] Rasmussen, C.., Williams, C.K.. (2006). Gaussian Processes for Machine Learning, the MIT Press, Massachusetts Institute of Technology.
[41] The MathWorks Inc. The MathWorks Inc.(2022). Statistics and Machine Learning Toolbox (R2022a).
[42] Vapnik, V.N. (1995). The Nature of Statistical Learning Theory, Springer New York, NY.
[43] Plevris, V., Solorzano, G., Bakas, N., Seghie, M.E.A. Ben. (2022). Investigation of performance metrics in regression analysis and machine learning-based prediction models, 8th Eur. Congr. Comput. Methods Appl. Sci. Eng. DOI: 10.23967/eccomas.2022.155.
[44] MATLAB. (2022). Version 9.12.0.2009381 (R2022a), Natick, Massachusetts, The MathWorks Inc.